

Article

Direct Energy Deposition of TiAl for Hybrid Manufacturing and Repair of Turbine Blades

Silja-Katharina Rittinghaus ^{1,*}, Janett Schmelzer ² , Marcus Willi Rackel ³, Susanne Hemes ⁴, Andreas Vogelpoth ¹, Ulrike Hecht ⁴ and Andreas Weisheit ¹

¹ Fraunhofer Institute for Laser Technology (FhG-ILT), 52074 Aachen, Germany; andreas.vogelpoth@ilt.fraunhofer.de (A.V.); andreas.weisheit@ilt.fraunhofer.de (A.W.)

² Otto-von-Guericke-Universität Magdeburg, Institut für Werkstoff und Fuegetechnik, 39106 Magdeburg, Germany; janett.schmelzer@ovgu.de

³ Helmholtz-Zentrum Geesthacht, 21502 Geesthacht, Germany; marcus.rackel@hzg.de

⁴ Access e.V, 52072 Aachen, Germany; s.hemes@access-technology.de (S.H.); u.hecht@access-technology.de (U.H.)

* Correspondence: siljakatharina.rittinghaus@ilt.fraunhofer.de; Tel.: +49-241-8906-8138

Received: 21 August 2020; Accepted: 9 September 2020; Published: 1 October 2020



Abstract: While repair is mainly used to restore the original part geometry and properties, hybrid manufacturing aims to exploit the benefits of each respective manufacturing process regarding either processing itself or resulting part characteristics. Especially with the current implementation of additive manufacturing in the production of TiAl, turbine blades for both hybrid manufacturing and repair new opportunities are enabled. One main issue is the compatibility of the two or more material types involved, which either differ regarding composition or microstructure or both. In this study, a TNMTM-alloy (Ti-Nb-Mo) was manufactured by different processes (casting, forging, laser additive manufacturing) and identically heat-treated at 1290 °C. Chemical compositions, especially aluminum and oxygen contents, were measured, and the resulting microstructures were analyzed with Scanning Electron Microscopy (SEM) and High-energy X-ray diffraction (HEXRD). The properties were determined by hardness measurements and high-temperature compression tests. The comparison led to an overall assessment of the theoretical compatibility. Experiments to combine several processes were performed to evaluate the practical feasibility. Despite obvious differences in the final phase distribution caused by deviations in the chemical composition, the measured properties of the samples did not differ significantly. The feasibility of combining direct energy deposition (DED) with either casting or laser powder bed fusion (LPBF) was demonstrated by the successful build of the dense, crack-free hybrid material.

Keywords: titanium aluminides; additive manufacturing; microstructure; phase distribution; mechanical properties

1. Introduction

Due to suitable high-temperature properties, such as high specific high-temperature strength (100–150 MPa cm³/g), high specific rigidity (35–42 GPa cm³/g), high oxidation, and creep resistance, intermetallic γ titanium aluminide alloys with a density of $\rho = 3.9\text{--}4.1$ g/cm³ are considered to be substitutes for nickel-based superalloys with approximately twice the density ($\rho = 7.9\text{--}8.5$ g/cm³) [1,2]. The limited ductility and fracture toughness of the material [3,4], as well as the high reactivity of titanium, especially with oxygen, water, and nitrogen, are challenging both for the use and the production of titanium aluminide components. Applications are mainly in the aerospace industry and, in some cases, in the automotive and energy sectors [1,3]. One of the main applications is the use of low-pressure

turbine blades at an operating temperature of approx. 700 °C. The best-known alloys currently in service are GE4822 (Ti-48Al-2Nb-2Cr, at.%), a two-phase TiAl alloy used by GE Aviation/Avio Aero in the GE90, CFM International LEAP (formerly LEAP X) and GEnX engines, and the TNM-B1 (B1 = 0.1 wt.-% B) [5]. TNMTM is a group of forging alloys fully solidified through the β phase and protected by MTU Aero Engines AG. Leistriz Turbinentechnik GmbH uses it to manufacture low-pressure turbine (LPT) blades [5], which are installed in the geared turbofan PW1110G. The target element distribution of the main alloy elements is adjusted according to the desired distribution of the three phases— α_2 , γ , and β/β_0 (B2) [1]—and is in the range Ti(42-44)Al-(3-5)Nb-(0.1-2)Mo-(0.1-0.2)B (in at.%).

The alloy investigated in this paper is designated TNM-B1. The nominal composition may differ, and the one used here is Ti-43.5Al-4Nb-1Mo-0.1B (in at.%) [6]. The density is 4.16 g/cm³. The alloy solidifies via the β phase by means of β phase stabilizing elements, such as Mo and Nb [7]. Diffusion processes in the α_2 and γ phase are crucial for heat treatment results and slowed down by Nb. An increase in the activation energy of diffusion in these phases is achieved by the addition of Mo [8]. Both serve to improve the creep properties. Boron is added in the range of 0.1–1 at% due to its grain refining and texture-reducing effect [2,4,7]. The addition of boron leads to the formation of stable Ti-boride precipitates, which also inhibit grain growth during heat treatment.

Casting and forging processes are established for production, which are very complex due to the low ductility and fracture toughness as well as the high oxygen affinity of the intermetallic material. The industry's interest in the tool-free additive production of titanium aluminide components is, therefore, great. Functional tests, e.g., at GE Avio Aero with blades manufactured by additive electron beam melting (EBM), are already being carried out [9]. Other approaches in research include powder metallurgy (PM) via hot isostatic pressing (HIP) [10], metal injection molding (MIM) [11], or spark plasma sintering (SPS) [12]. With the increasing use of γ -TiAl in aircraft turbines, the need for repair or modification solutions will increase, irrespective of the original production route of the components concerned. Currently, the research is performed on transient liquid phase (TLP) bonding for the repair of γ -TiAl, using Fe or Ni as melting point depressing elements (MPD) [13]. Furthermore, in the recently completed LuFo-project (FKZ 20T1526A), the diffusion welding of TiAl was investigated with, again, the aim of the repair.

With direct energy deposition (DED), components can not only be built up additively but also be repaired near net-shape. The suitability of DED as an additive manufacturing process for coating and repair tasks has already been proven for numerous material groups (nickel-based alloys, steel materials, etc.). Especially the ability to build on 3D surfaces enables DED as a potential method to individualize parts manufactured via a different route.

Crack-free processing of titanium aluminides with DED is possible by preheating the substrate during the process [14–18]. The temperature of the substrate or the already built-up volume required to produce crack-free traces must be in the brittle-ductile transition range (550–800 °C) for Ti-based alloys [19]. The actual preheating temperature required depends on the alloy, the geometry, and the process parameters. To protect the melt from oxidation, the process zone is shielded locally with inert gas [15] or a global inert gas atmosphere [17,20–24] with < 100 ppm [20] or even smaller amounts of O [25]. The oxygen content after DED has been measured in [26,27] at approx. 500–1200 ppm with complete shielding. The influence of process conditions and process parameters on the oxygen content in the material produced has hardly been investigated so far [27], and the contents of <1000 ppm O in DED GE4822 and TNM-B1 have been documented in some publications [15,25,28].

According to [29], phase transformations can be achieved for TNM at temperatures between 1230 °C and 1300 °C, depending on the composition and thus, for example, the aluminum content. In [30], results are published on the influence of heat treatment temperature, duration, and cooling rate. A typical composition for a TNM type alloy (MTU/Pratt Whitney) is approximately 79% γ , 25% α_2 , and 5% β [31]. However, the heat treatment methods applied in the literature vary widely. Thus, a direct comparison of the microstructure and properties is hardly possible but crucial to determine whether materials from the same alloy are compatible, as the final part can be treated only as a whole.

Following this approach, samples in this work produced with different manufacturing methods, including conventional as well as additive manufacturing, were identically heat treated. The material was examined regarding microstructure and properties, taking into account the respective chemical composition. It was experimentally demonstrated that DED combined with cast and laser powder bed fusion (LPBF) resulted in dense, crack-free samples, which were analyzed as well. The properties of γ -TiAl produced with DED in the investigations carried out corresponded overall to those achieved with processes used to produce components made of γ -TiAl. DED was, therefore, suitable as a process for processing γ -TiAl. However, the oxygen content was still above the critical value of 1000 ppm, which reduced the ductility, especially at room temperature, and thus made reworking and assembly of components even more difficult.

2. Materials and Methods

2.1. Materials

The powder materials used in this work, made of the alloy TNM-B1, were produced by TLS Technik GmbH Spezialpulver KG (Bitterfeld-Wolfen, Germany) via the EIGA process with argon gas atomization. The used particle size distribution was 20–90 μm (DED) and 20–80 μm (LPBF), respectively. Since Al and O have a significant influence on the microstructure evolution, the content of both elements was measured for the two powder batches. The powder contained 820 ppm O and 29.5 wt.-% Al (DED) and 850 ppm O and 29.3 wt.-% Al (LPBF). DED samples were built on similar TNM substrate material with a thickness of 4 mm (produced by Access e.V., Aachen, Germany). The substrates were produced by investment casting and were used in the non-heat-treated cast state. LPBF samples were built on Ti6Al4V material.

2.2. Additive Manufacturing

2.2.1. Direct Energy Deposition (DED) of TiAl

Tests for DED were carried out on a 3-axis CNC portal system in a laboratory setup. A 2 kW diode laser of the type LDF2000 ($\lambda = 1025$ and 1064 nm) from Laserline GmbH (Muelheim-Kaerlich, Germany) was used as a laser beam source. As for focusing optic, an optical system of the OTS 5 series from Laserline GmbH (focal length 182 mm) was used. The powder was conveyed by a conveyor from GTV Verschleißschutz GmbH (Luckenbach, Germany). The process parameters used for DED are listed in Table 1.

Table 1. The process parameters for DED (Direct Energy Deposition) of TNMTM (Ti-Nb-Mo) [32].

| Beam Diameter | Laser Power | Scanning Velocity | Offset (z) |
|---------------|-------------|-------------------|------------|
| 0.6 mm | 66 W | 500 mm/min | 0.25 mm |

The complete experimental setup was located inside a protective gas chamber (glovebox), which was closed completely airtight and filled with Argon 4.6 (50 ppm O). Preheating up to 900 °C was conducted by induction heating.

2.2.2. Laser Powder Bed Fusion (LPBF) of TiAl

The system used was a laboratory LPBF system equipped with a multi-mode fiber laser with a maximum laser power of 500 W. The focus diameter of the beam was 100 μm . Argon was used as protective gas. The oxygen concentration in the process chamber was < 10 ppm. The process parameters are listed in Table 2.

Table 2. The process parameters for LPBF (Laser Powder Bed Fusion) of TNMTM.

| Beam Diameter | Laser Power | Scanning Velocity | Layer Thickness |
|---------------|-------------|-------------------|-----------------|
| 0.09 mm | 200 W | 1200 mm/s | 0.03 mm |

The system was equipped with an induction preheating system, with which the substrate could be heated up to 1600 °C. The preheating temperature applied was 900 °C.

2.3. Heat Treatment

Heat treatment was performed at 1290 °C for one hour, followed by furnace cooling. The cooling rate was approximately 4 K/min. To minimize surface oxidation, a continuous argon gas stream of 300 L/h was used.

2.4. Analytical Methods

2.4.1. Chemical Composition

Oxygen contents were determined with carrier gas hot extraction. Aluminum and other elements were measured with ICP-OES, according to DIN 51008-2 and DIN 51009.

2.4.2. Microstructure and Phase Analysis

Samples for microstructure analysis were cut from the build-up volumes, and the cross-sections were prepared parallel to the build direction (*z*). A ZeissULTRA55 SEM (Carl Zeiss Microscopy GmbH, Jena, Germany) with field-emission gun (= FE-SEM) was used for imaging. An Oxford-TETRA-BSE (= back-scattered-electron) detector (Oxford Instruments, Abingdon, UK) was used for micrographs, and the measurements were made at 15 kV.

High-energy X-ray diffraction (HEXRD) measurements were performed at DESY (Deutsches Elektronen-Synchrotron), Hamburg, Germany. The High-Energy Materials Science Beamline (HEMS/P07) operated by Helmholtz-Zentrum Geesthacht at the PETRA III synchrotron radiation facility was used. The specimens were measured in transmission with a beam size of 1 mm by 1 mm, photon energy of 100 keV ($\lambda = 0.1240 \text{ \AA}$), and an exposure time of 0.1 s. The Debye-Scherrer diffraction rings were recorded on a Perkin Elmer XRD 1622 flat panel detector (PerkinElmer Inc., Santa Clara, CA, USA). For calibration, a measurement with a standardized lanthanum hexaboride (LaB₆) powder was used in order to calculate the instrumental parameters, the beam center, and the sample-detector distance. The phase fractions were calculated with the Rietveld analysis software package MAUD (Version 2.92, L. Lutterotti, University of Trento, Italy).

2.4.3. Mechanical Properties

Vickers hardness was tested with a load of 30 kgf and a loading time of 15 s. Test specimens for compression tests of the dimensions $5 \times 3 \times 3 \text{ mm}^3$ were cut out of larger samples by eroding. The tests were carried out parallel to the build direction. Compression tests were performed uniaxially on a Zwick Roell Z100 (ZwickRoell GmbH & Co. KG, Ulm, Germany), equipped with a furnace from Maytec Mess- und Regeltechnik GmbH (Singen, Germany) at 700 °C under argon. The speed during compression tests was 10^{-4} mm/s until breakage.

3. Results

3.1. Chemical Composition

In Table 3, the chemical compositions of the samples used for tests are listed. Cast and forged samples were intentionally selected to have a higher oxygen content than technically possible so that the oxygen contents were similarly high for all samples, and the influence of the manufacturing route

on the phase formation after heat treatment could be investigated. Significant differences can be seen in the aluminum content, which was at around 0.4 wt.% lower for LPBF, cast, and forged material than in the DED sample.

Table 3. Chemical composition of TNM-B1 samples; values in wt.-%.

| Sample | Ti | Al | Nb | Mo | B | O ¹ |
|---------|-------|-------|------|------|-------|----------------|
| DED | 58.59 | 29.14 | 9.6 | 2.15 | 0.038 | 2130 |
| LPBF | 60.38 | 28.67 | 8.26 | 2.06 | 0.036 | 1770 |
| Cast | 60.41 | 28.19 | 8.85 | 2.24 | 0.021 | 1750 |
| Forging | 60.32 | 28.35 | 8.73 | 2.19 | 0.025 | 2070 |

¹ values given in ppm.

In comparison with LPBF, the Al content of the powder material used for DED was already higher (29.5 and 29.3 wt.-%, respectively). Additionally, the aluminum loss due to evaporation was likely lower due to the lower mean melt temperature. For forged material, no further influence of the manufacturing process on the composition was given as no molten phase was involved in the process.

3.2. Microstructure and Phases

3.2.1. Microstructure

In Figure 1, SEM images of the investigated material samples in the heat-treated condition are shown. All samples showed a density > 99.8%, determined by metallographic analysis, and were free of cracks. The microstructure consisted of lamellar grains ($\alpha_2 + \gamma$ colonies), inter-crystalline γ grains, and BCC-B2 (β_0) phase fractions. The phases could be distinguished from each other by their gray-scale value: α_2 (gray), γ (dark gray), and β_0 (light gray/white).

Two transition temperatures were important in the heat treatment of γ -TiAl. The α -transus temperature $T_{\alpha\text{-transus}}$ (partly identical with the γ solvus temperature ($T_{\gamma\text{-solvus}}$) [33]) was the temperature at which the formation of the γ phase began during cooling or at which (ordered) α and γ were dissolved during heating. Thus, by heat treatment above $T_{\alpha\text{-transus}}$, completely lamellar structures could be achieved on cooling. In addition, complete γ solution favored grain growth of the α phase, which was inhibited by the still existing γ phase. During heat treatment in the $\alpha_2 + \gamma$ phase region, characterized by temperatures between $T_{\alpha\text{-transus}}$ and the eutectoid temperature T_e , almost lamellar to duplex structures were produced. The closer the heat treatment temperature was to T_e , the greater the proportion of γ [34–36].

The eutectoid transformation for TNM with the nominal composition of Ti-43.5Al-4Nb-1Mo-0.1B (at.-%) occurred at $T_e = 1160$ °C, and the α to γ transformation temperature $T_{\alpha\text{-transus}}$ was 1250 °C. The respective transformation temperatures were sensitive to the aluminum content. Lower aluminum contents shifted the phase equilibrium towards a higher $T_{\alpha\text{-transus}}$. With regard to the effect of oxygen on the solid-state transformation, the ordered α_2 phase was stabilized against the α phase at least in binary alloys, so that the order of the α phase to α_2 could start at higher temperatures, even before γ was formed. This could result in smaller lamella distances, which stabilized the lamellar structure of the $\alpha_2 + \gamma$ colonies. Due to the preferred order of α_2 compared to γ , the resulting α_2 phase fraction was increased by higher oxygen contents [37–40]. Due to large differences in oxygen solubility between the α_2 and γ phase, the conversion from α to γ was significantly slowed down.

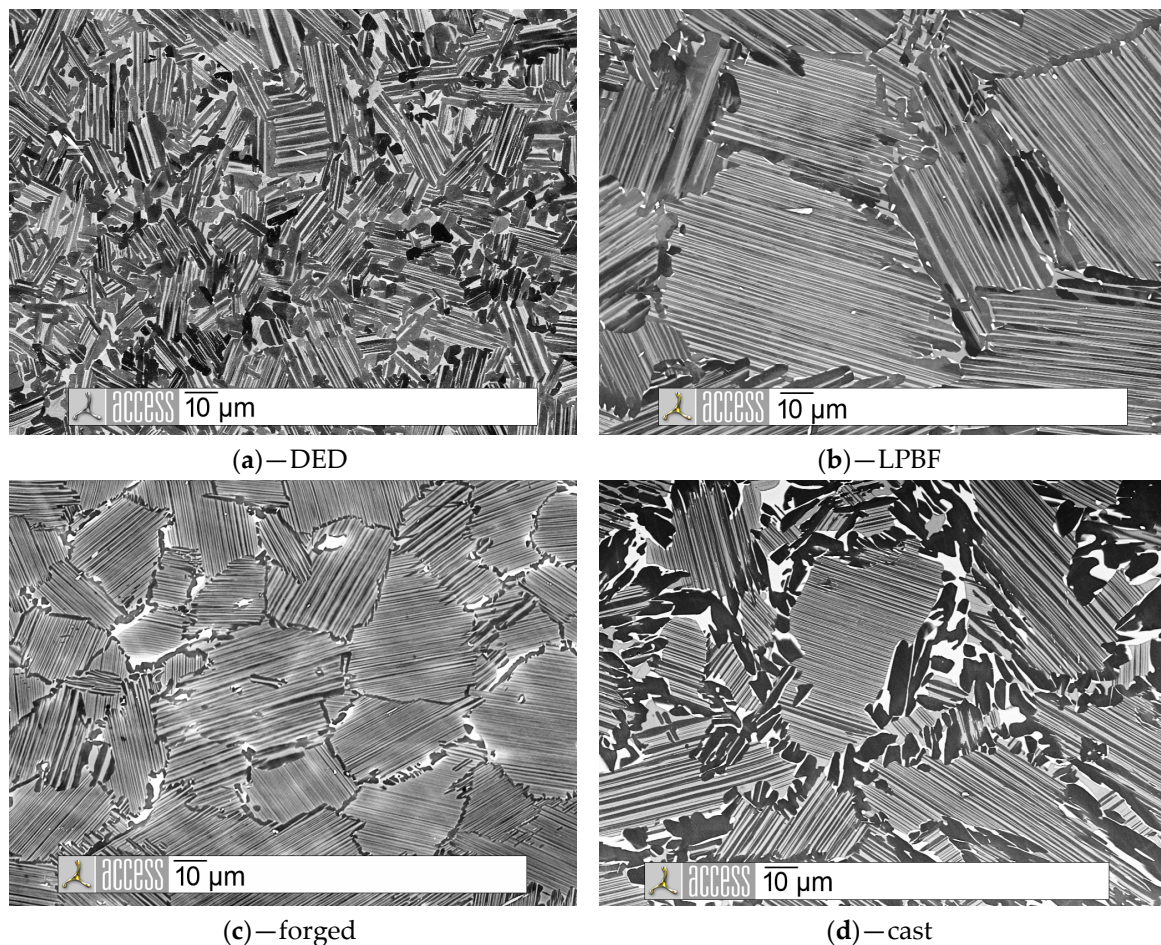


Figure 1. SEM images of heat-treated TNM (a) manufactured by DED; (b) manufactured by LPBF [32]; (c) manufactured by forging; (d) manufactured by casting.

During heat treatment at 1290 °C, the γ phase was solved when $T_{\gamma\text{-solvus}}$ was reached. When cooling from the ($\alpha + \beta$) phase field, the known solid-state transformations took place. Again, γ lamellae were formed from supersaturated α grains [41]. During further cooling, due to the phase imbalance, supersaturated α_2 grains segregated to lamellar α_2/γ colonies. At the same time, a reaction according to $\alpha_2 \rightarrow \beta_0 + \gamma$ took place, also to compensate for the phase imbalance. The γ lamellae coarsened until they formed globular γ grains. The main driving force for the forming process is the minimization of interfacial energy [42]. At low cooling rates, α_2 grains were not supersaturated, and the formation of the fine-lamellar structures did not occur. In Figure 1a, as described in [30], parts of coarse γ lamellae are visible. From this, it can be concluded that for DED samples, the γ phase had not been completely dissolved, and, therefore, the local $T_{\gamma\text{-solvus}}$ temperature was >1290 °C. The increase in $T_{\gamma\text{-solvus}}$ could be attributed to (locally) higher Al contents or increased oxygen contents. Residues of α_2 grains were coherent with the comparatively slow cooling during furnace cooling. The boundaries of the lamellar $\alpha_2+\gamma$ grains in the heat-treated cast sample, depicted in Figure 1d, were also occupied by γ and β_0 phase. The heat treatment temperature of 1290 °C was thus also for the elemental composition of the cast material, despite the low Al content, locally below $T_{\gamma\text{-solvus}}$. The same was valid for the microstructure of the forged sample in Figure 1c. The morphology of the γ grains was slightly different from the cast state; due to the forging process, some grains were elongated. In comparison, the microstructure of the LPBF samples (Figure 1b) was almost completely lamellar, and some grain boundary areas with globular γ phase and very small portions β_0 were present. The heat treatment temperature (1290 °C) was, therefore, $\geq T_{\gamma\text{-solvus}}$ for the large, completely lamellar microstructure components of the LPBF material.

Overall, Figure 1 implies that except for the LPBF sample, all samples were heat treated in the ($\alpha + \gamma$) phase field, and $T_{\gamma\text{-solvus}}$ was not exceeded at least proportionally. The composition alone didn't deliver a valid argument for this exception. From this, it can be deduced that the transformation processes during the heat treatment were also significantly influenced by the very fine LPBF microstructure in the as-built condition. The original grain size is about 1–7 μm diameter and, thus, approximately 1/3 the size of DED and 10 times smaller compared to cast [28]. Many interfaces and short diffusion paths thus represented an essential influencing variable.

3.2.2. Phase Composition

In Table 4, measurement results from the synchrotron HEXRD investigation are listed. All materials investigated showed at least three phases, with significant differences in the respective phase distribution, despite the chemical similarity of the materials.

Table 4. The phase composition of heat-treated TNM-B1 samples; values in vol.-%.

| Sample | α_2 /(O) | γ | β_0 /(ω_0) |
|---------|-----------------|----------|---------------------------|
| DED | 22.9 | 75.8 | 1.3 |
| LPBF | 40.6 | 57.4 | 2.0 |
| Cast | 29.5 | 63.9 | 6.6 |
| Forging | 34.7 | 57.7 | 7.6 |

The γ phase fraction in DED samples was higher than in LPBF, cast, and forged samples. The β_0 phase content in both LPBF and DED samples was smaller than in cast or forged samples. This went along with the observations from Figure 1 and, together with Table 3, suggested a correlation between γ phase and aluminum content, on the one hand, and fineness of the structure and β_0 phase fraction, on the other. However, local fluctuations in the chemical composition and smaller differences in the fineness of the microstructure, which are also present in the other material samples, must be considered to a limited extent. The formation of γ grains is generally favored because of the discontinuous coarsening in fine-grained structures, which is described in, e.g., [43].

In addition to the aforementioned, the existence of further phases (O and ω_0) can be read from the diffractograms in Figure 2. Both phase fractions were very small, and a clear separation for quantification was not possible because of overlapping peaks of the crystallographic-related phases.

The ω_0 phase was formed as nanoscale precipitations from β/β_0 at temperatures around 900 °C. During heating up, the ω_0 phase dissolved in the temperature range of 930–960 °C, and the β_0 phase was present [33]. The orthorhombic O phase was visibly formed from α_2 -phase at temperatures below 660 °C, remained stable up to that temperature, and was associated with improved room temperature ductility [44,45]. The O phase was dissolved again at about 700 °C. The occurrence of both phases could be explained by cooling during heat treatment. By slow furnace cooling with approx. 4 K/s, the material reached the respective temperature range of the formation of the ω_0 and O phase for a sufficiently long time. Since the α_2 -phase fraction in DED material was relatively small compared to the other samples, the associated O phase formation didn't take place to a detectable amount. The same could be derived for the ω_0 phase, whose occurrence was observed in the samples with a comparatively high β -content produced by casting and forging.

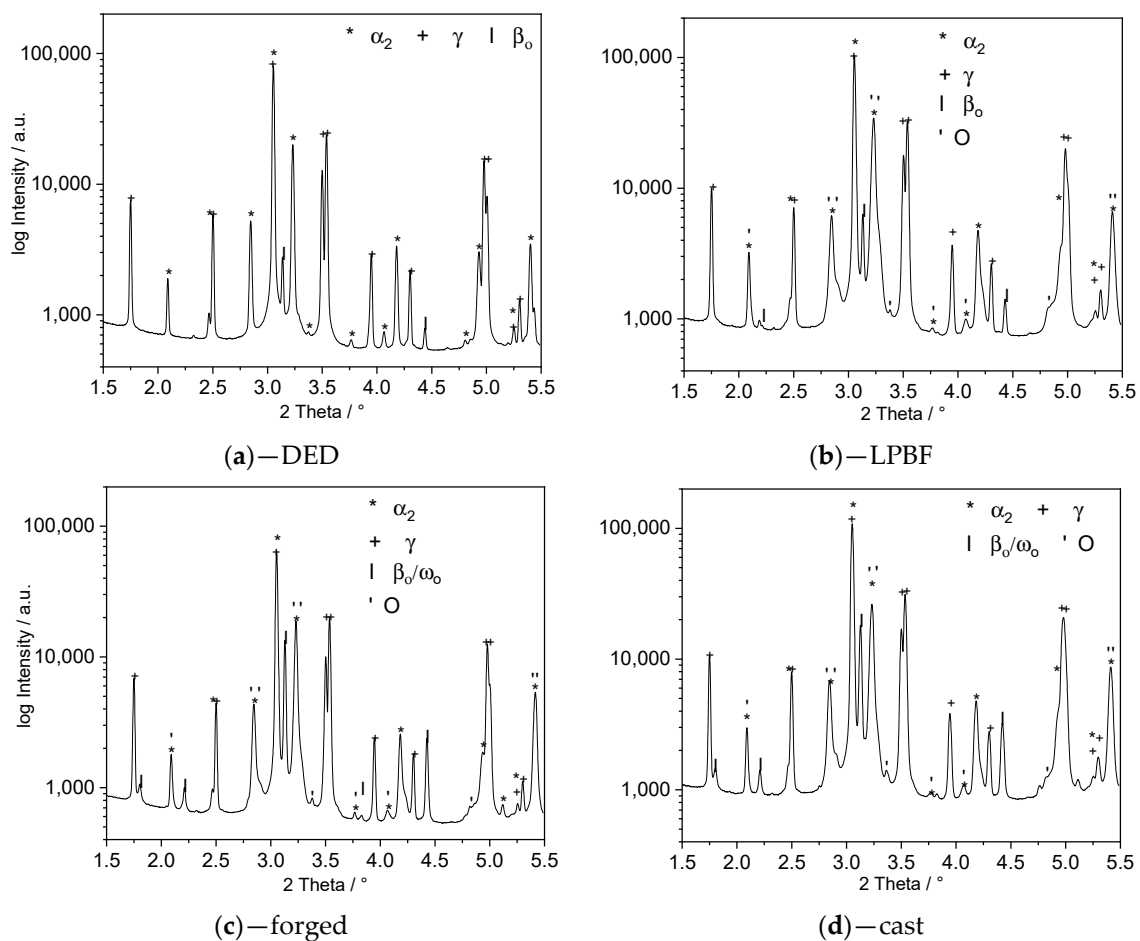


Figure 2. Diffraction patterns of heat-treated TNM (a) manufactured by DED; (b) manufactured by LPBF; (c) manufactured by forging; (d) manufactured by casting.

3.3. Mechanical Properties

High-Temperature Compressive Strength

In Table 5, the results of the compression tests, performed at 700 °C on three samples each, are listed.

Table 5. Compressive strength of TNM-B1 samples at 700 °C.

| Sample | Compressive Yield Strength $S_{d0.2}$ | Fracture Strength S_B | Compression at Break A_t |
|---------|---------------------------------------|-------------------------|----------------------------|
| DED | 566 MPa \pm 23 | 1190 MPa \pm 44 | 24.0 % |
| LPBF | 465 MPa \pm 49 | 1237 MPa \pm 10 | 15.1 % |
| Cast | 551 MPa \pm 22 | 1219 MPa \pm 15 | 15.4 % |
| Forging | 567 MPa \pm 15 | 1210 MPa \pm 15 | 15.4 % |

It can be seen that, on average and taking into account the deviation, both compressive strength, measured on the basis of the fracture strength, and ductility of the DED specimens were comparable with the characteristic values of the cast and forged specimens. The range of elastic deformation ended consistently at approx. 500–550 MPa $S_{d0.2}$. The fracture strength S_B was approx. 1150–1200 MPa. The fracture compression A_t of all materials except for the DED specimens was approx. 15.3%. The comparatively greater fracture compression of the material built up with DED could be attributed to the fine-grained nature of the material, as it can be seen from Figure 1. This, again, was highly dependent on the parameters used for the sample production [32].

3.4. Repair and Hybrid Manufacturing

3.4.1. Feasibility

In Figure 3, photographs of hybrid samples are presented. These showed the feasibility of repair and hybrid manufacturing of γ -TiAl.

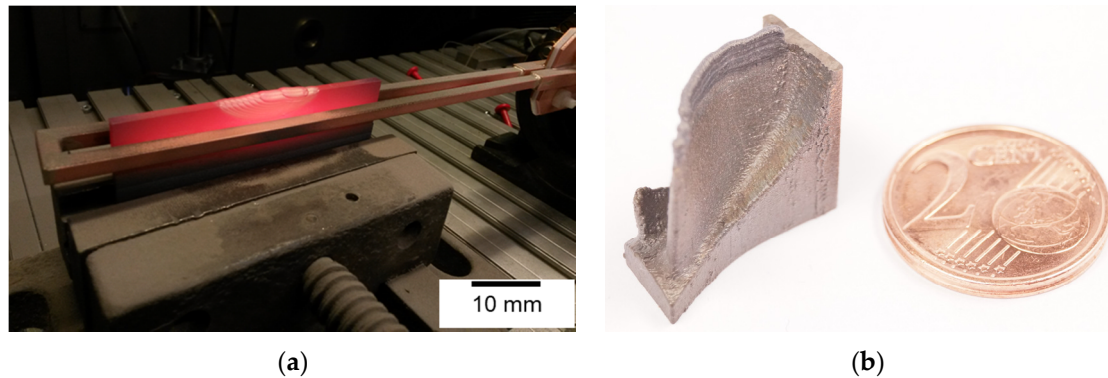


Figure 3. Photographs of hybrid γ -TiAl samples. (a) DED and cast, (b) DED and LPBF.

In Figure 3a, a mockup cast part with a DED repaired section is depicted in as-built condition, cooling down immediately after the process. In Figure 3b, a section of an LPBF turbocharger wheel with a DED tip is presented to demonstrate the possible combination of these processes as well.

3.4.2. Microstructure of Hybrid Materials

For further investigation, hybrid samples consisting of a cast base and a DED upper section of a total size of 60 mm (length) \times 20 mm (height) \times 4 mm (width) were produced, heat-treated, and analyzed. In Figure 4, SEM images of the transition zone between the cast (bottom) and DED (top) material in heat-treated conditions are depicted.

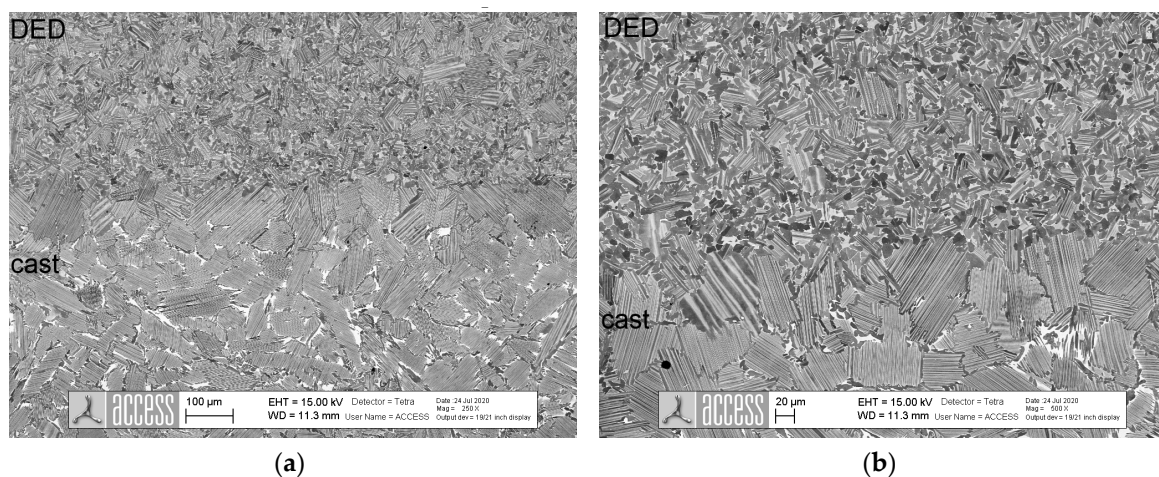


Figure 4. SEM images of the transition zone between cast and DED material in heat-treated condition (a) 100 \times ; (b) 500 \times magnification.

The materials could be clearly distinguished by their grain sizes and phases. The lamellar grains at the direct transition (heat affected zone) also appeared larger than those of the pure cast material. The heat influence of the application of the first DED layers was, therefore, large enough to activate grain growth already during the build-up process. Stresses were well absorbed by the material; no crack formation occurred.

3.4.3. Micro Indentation of Hybrid Materials

In Table 6, the results of the micro indentation tests, performed on four hybrid samples with three indents each, are listed. Despite the generally high scattering, higher hardness values were measured in the cast material.

Table 6. Microhardness HV-30 of TNM-B1 samples.

| Zone | Mean Value | Standard Deviation |
|--------|------------|--------------------|
| DED | 347 | 22 |
| Hybrid | 387 | 28 |
| Cast | 383 | 27 |

In Figure 5, an exemplary SEM image of the test zone of one hybrid sample is added. The transition area itself was rather small at approx. 200 μm and could be identified by the differences between the grain sizes.

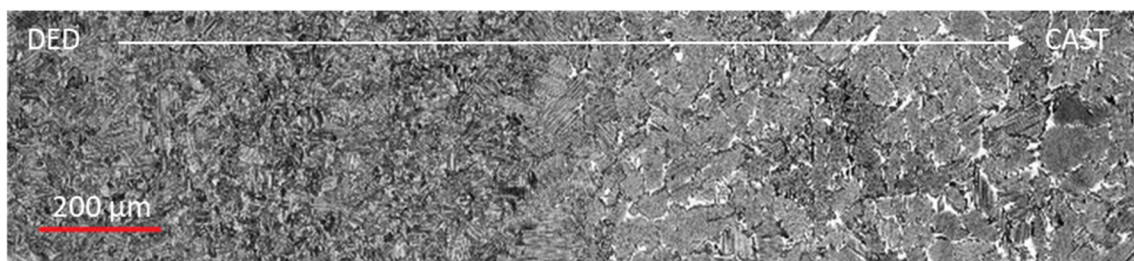


Figure 5. Micro indentation test zone of hybrid γ -TiAl samples. DED (left) and cast (right).

An explanation was provided by the proportion of (fine) lamellar areas in the test surface, which was significantly larger in the cast material. DED material had superfine lamellae as well as very small grain sizes. Both spoke for high hardness values. As the test indentations were relatively large, the probability of hitting purely lamellar grains was higher in the cast material, so that, on average, the softer phases were measured in the DED area. In the hybrid zone, the proportion of the β phase was again somewhat smaller than in the cast area, so that the hardness was still slightly higher, but just as high as in the cast material when deviations were taken into account.

4. Discussion

The high-temperature compressive strength (700 $^{\circ}\text{C}$) of DED-manufactured material is approx. 1200 MPa, which is also comparable to that of the identically heat-treated cast, forged, and LPBF material. The biggest differences are found in the almost non-existent β_0 phase and an approx. 15% higher γ phase content compared to cast, forged, and LPBF material, which can be attributed to an approx. 0.4% higher aluminum content of the DED samples. Since the oxygen content of all tested materials is similarly high at approx. 2000 ppm, this can be ruled out as the main cause of the differences between the materials. The overall low strength values for TNM-B1 can be explained both by the possibly less favorable heat treatment and the high oxygen content. Thus, the properties of γ -TiAl produced with DED correspond, in the context of the investigations carried out, overall to those achieved with processes used to produce components made of γ -TiAl.

The oxygen content of all samples is above the limit value of 1200 ppm. This allows for a more specific analysis of other influences in this study but is known to be too high for application purposes [46]. The ductility, especially at room temperature, is highly influenced by O, which is detrimental for at least any post-processing. For cast and thus forged material, O contents are regularly lower, usually well below 800 ppm [47]. Samples with higher content are deliberately selected in order to make the composition comparable and to be able to observe the influence of the different temperature-time

curves of the production routes. For AM (Additive Manufacturing), the processing steps of powder production and the additive manufacturing itself will always lead to an unavoidable increase in oxygen. However, EBM (Electron Beam Melting) already allows us to minimize the uptake during AM close to zero due to the vacuum, which is why it is the most frequently selected AM method for processing γ -TiAl. At the same time, aluminum loss is comparatively higher [48]. The resulting EBM microstructures [49], are quite like the ones achieved with LPBF in this work, which suggests a transferability of the results shown.

The hardness of hybrid DED and cast samples varies measurably depending on the test area.

Contrary to other measurements, the hardness of the cast area is higher than that of the DED area in this test [30,32]. Due to the small grain sizes of the three-phase DED material, the positioning and size of the measuring points are particularly important. The transition zone shows the high lamellar microstructure of the cast with partly smaller grain sizes of DED so that there is a tendency to slightly higher hardness.

Due to the similarity of the material properties and the flawless transition zones, DED is generally suitable to be combined with AM, casting, or forging. The ability to build on 3D structures allows for repair and modification or individualization of series production parts likewise.

5. Conclusions

The investigated DED samples differ uniformly from material samples produced by other methods in that their aluminum content is at least 0.4% higher, which can easily be balanced when considered in the powder production process. As a consequence, the DED $T_{\gamma\text{-solvus}}$ temperature is increased. Therefore, the selected heat treatment (1290°, 1 h, FC) is carried out at too low a temperature to completely equalize the microstructure of TNM-B1 materials of different production routes. This is likely to be improved with an increase in the heat treatment temperature. However, despite the differences in microstructure, the mechanical properties are quite similar to a fracture strength of approx. 1200 MPa.

The process-related feasibility of combining DED with other manufacturing methods in a hybrid process is demonstrated. The results overall imply that DED can likely be used as a repair and hybrid manufacturing technique for γ -TiAl parts. Interesting in the future and a consistent next step towards industrial implementation are investigations of mechanical properties of such compounds, the targeted adjustment of which can represent a further step towards the more efficient exploitation of material properties.

Author Contributions: Conceptualization: S.-K.R.; methodology: S.-K.R.; validation: S.-K.R., J.S., S.H., A.V.; investigation: S.-K.R., J.S., M.W.R., S.H.; writing—original draft preparation: S.-K.R.; writing—review and editing, A.W., U.H.; visualization: S.-K.R.; funding acquisition: A.W., U.H. All authors have read and agreed to the published version of the manuscript.

Funding: This research was partially funded by the Federal Ministry of Economics and Energy, grant number 20T1311.

Acknowledgments: We acknowledge DESY (Hamburg, Germany), a member of the Helmholtz Association HGF, for the provision of experimental facilities. Parts of this research were carried out at PETRA III, P07 High-Energy Materials Science Beamline, and we would like to thank Norbert Schell and Andreas Stark for assistance.

Conflicts of Interest: The authors declare no conflict of interest. The funders had no role in the design of the study; in the collection, analyses, or interpretation of data; in the writing of the manuscript, or in the decision to publish the results.

References

1. Leyens, C.; Peters, M. *Titan und Titanlegierungen*, 3rd ed.; Wiley-VCH: Weinheim, Germany, 2002; ISBN 9783527305391.
2. Wessel, W. Mikrostrukturelle Untersuchungen der Rissinitiierung und-Ausbreitung in Intermetallischen TiAl-Legierungen unter Zyklischer und Quasistatischer Belastung. Ph.D. Thesis, Kassel University, Kassel, Germany, 24 November 2011.

3. Ferro, R.; Saccone, A. *Intermetallic chemistry*, 1st ed.; Pergamon: Oxford, UK, 2008; ISBN 9780080553351.
4. Appel, F.; Paul, J.D.H.; Oehring, M. *Gamma Titanium Aluminide Alloys: Science and Technology*; Wiley-VCH: Weinheim, Germany, 2011; ISBN 9783527315253.
5. Janschek, P. Wrought TiAl Blades. *Mater. Today Proc.* **2015**, *2*, 92–97. [[CrossRef](#)]
6. γ -TiAl TNM®-B1 Ingots. Available online: <https://www.gfe.com/produktbereiche/titaluminide/produktuebersicht/> (accessed on 2 August 2019).
7. Bolz, S.; Oehring, M.; Lindemann, J.; Pyczak, F.; Paul, J.; Stark, A.; Lippmann, T.; Schrüfer, S.; Roth-Fagaraseanu, D.; Schreyer, A.; et al. Microstructure and mechanical properties of a forged β -solidifying γ TiAl alloy in different heat treatment conditions. *Intermetallics* **2015**, *58*, 71–83. [[CrossRef](#)]
8. Clemens, H.; Wallgram, W.; Kremmer, S.; Güther, V.; Otto, A.; Bartels, A. Design of Novel β -Solidifying TiAl Alloys with Adjustable β /B2-Phase Fraction and Excellent Hot-Workability. *Adv. Eng. Mater.* **2008**, *8*, 707–713. [[CrossRef](#)]
9. Varetti, M. *Design and Turbine Architectures: AM Enabling Technologies*; ICTM: Aachen, Germany, 2015.
10. Schloffer, M.; Iqbal, F.; Gabrisch, H.; Schwaighofer, E.; Schimansky, F.P.; Mayer, S.; Stark, A.; Lippmann, T.; Göken, M.; Pyczak, F.; et al. Microstructure development and hardness of a powder metallurgical multi phase γ -TiAl based alloy. *Intermetallics* **2012**, *22*, 231–240. [[CrossRef](#)]
11. Gerling, R.; Aust, E.; Limberg, W.; Puff, M.; Schimansky, F.P. Metal injection moulding of gamma titanium aluminide alloy powder. *Mater. Sci. Eng. A* **2006**, *423*, 262–268. [[CrossRef](#)]
12. Voisin, T.; Monchoux, J.-P.; Thomas, M.; Deshayes, C.; Couret, A. Mechanical Properties of the TiAl IRIS Alloy. *Metall. Mater. Trans. A* **2016**, *12*, 6097–6108. [[CrossRef](#)]
13. Hauschildt, K.; Stark, A.; Schell, N.; Müller, M.; Pyczak, F. The transient liquid phase bonding process of a γ -TiAl alloy with brazing solders containing Fe or Ni. *Intermetallics* **2019**, *106*, 48–58. [[CrossRef](#)]
14. Vilaro, T.; Kottman-Rexerodt, V.; Thomas, M.; Colin, C.; Bertrand, P.; Thivillon, L.; Abed, S.; Ji, V.; Aubry, P.; Peyre, P.; et al. Direct Fabrication of a Ti-47Al-2Cr-2Nb Alloy by Selective Laser Melting and Direct Metal Deposition Processes. *AMR* **2010**, *89*, 586–591. [[CrossRef](#)]
15. Thomas, M.; Malot, T.; Aubry, P. Laser Metal Deposition of the Intermetallic TiAl Alloy. *Metall. Mater. Trans. A* **2017**, *193*, 519–537. [[CrossRef](#)]
16. Brückner, F.; Finaske, T.; Willner, R.; Seidel, A.; Nowotny, S.; Leyens, C.; Beyer, E. Laser Additive Manufacturing with Crack-sensitive Materials. *LTI* **2015**, *2*, 28–30. [[CrossRef](#)]
17. Qu, H.P.; Li, P.; Zhang, S.Q.; Li, A.; Wang, H.M. Microstructure and mechanical property of laser melting deposition (LMD) Ti/TiAl structural gradient material. *Mater. Design* **2010**, *31*, 574–582. [[CrossRef](#)]
18. Cárcel, B.; Serrano, A.; Zambrano, J.; Amigó, V.; Cárcel, A.C. Laser Cladding of TiAl Intermetallic Alloy on Ti6Al4V—Process Optimization and Properties. *Phys. Procedia* **2014**, *56*, 284–293. [[CrossRef](#)]
19. Nacke, B.; Baake, E. (Eds.) *Induktives Erwärmen: Wärmen, Härten, Glühen, Löten, Schweißen*; Vulkan-Verlag: Essen, Germany, 2014; ISBN 978-3802723841.
20. Qu, H.P.; Li, P.; Zhang, S.Q.; Li, A.; Wang, H.M. The effects of heat treatment on the microstructure and mechanical property of laser melting deposition γ -TiAl intermetallic alloys. *Mater. Design* **2010**, *31*, 2201–2210. [[CrossRef](#)]
21. Srivastava, D.; Hu, D.; Chang, I.T.H.; Loretto, M.H. The influence of thermal processing route on the microstructure of some TiAl-based alloys. *Intermetallics* **1999**, *7*, 1107–1112. [[CrossRef](#)]
22. Wilden, J.; Frank, H.; Theiler, C.; Seefeld, T.; Sepold, G. Rapid Prototyping gerichtet erstarrter Titanaluminidstrukturen. In Proceedings of the 47th Internationales Wissenschaftliches Kolloquium, Ilmenau, Germany, 23–26 September 2002; p. 1.
23. Qu, H.P.; Wang, H.M. Microstructure and mechanical properties of laser melting deposited γ -TiAl intermetallic alloys. *Mater. Sci. Eng. A* **2007**, *466*, 187–194. [[CrossRef](#)]
24. Ocylok, S.; Weisheit, A.; Kelbassa, I. Increased Wear and Oxidation Resistance of Titanium Aluminide Alloys by Laser Cladding. *AMR* **2011**, *278*, 515–520. [[CrossRef](#)]
25. Rittinghaus, S.-K.; Weisheit, A.; Mathes, M.; Garcia Vargas, W. Laser Metal Deposition of Titanium Aluminides—A Future Repair Technology for Jet Engine Blades? In Proceedings of the 13th World Conference on Titanium, San Diego, CA, USA, 16–20 August 2015; pp. 1205–1211, ISBN 1119283264.
26. Srivastava, D.; Chang, I.T.H.; Loretto, M.H. The optimisation of processing parameters and characterisation of microstructure of direct laser fabricated TiAl alloy components. *Mater. Design* **2000**, *21*, 425–433. [[CrossRef](#)]

27. Srivastava, D.; Chang, I.T.H.; Loretto, M.H. The effect of process parameters and heat treatment on the microstructure of direct laser fabricated TiAl alloy samples. *Intermetallics* **2001**, *9*, 1003–1013. [[CrossRef](#)]
28. Rittinghaus, S.-K.; Vogelpoth, A. Laser additive manufacturing of titanium aluminides. In Proceedings of the Intermetallics 2017—Abstracts, Intermetallics Conference 2017, Bad Staffelstein, Germany, 2–6 June 2017; pp. 73–74.
29. Clemens, H.; Boeck, B.; Wallgram, W.; Schmoelzer, T.; Droessler, L.M.; Zickler, G.A.; Leitner, H.; Otto, A. Experimental Studies and Thermodynamic Simulations of Phase Transformations in Ti-(41–45) Al-4Nb-1Mo-0.1B Alloys. In Proceedings of the Materials Research Society MRS 2009, Materials Research Society MRS 2008 (Falls Meeting), Boston, MA, USA, 1–5 December 2008; pp. 115–120. [[CrossRef](#)]
30. Rittinghaus, S.-K.; Hecht, U.; Werner, V.; Weisheit, A. Heat treatment of laser metal deposited TiAl TNM alloy. *Intermetallics* **2018**, *95*, 94–101. [[CrossRef](#)]
31. Kim, Y.-W. Gamma Alloy Materials-Process-Microstructure Combinations for Greater Service Temperatures. In Proceedings of the TMS GAT-2017, San Diego, CA, USA, 26 February–2 March 2017.
32. Rittinghaus, S.-K. Laserauftragschweißen von γ -Titanaluminiden als Verfahren der Additiven Fertigung. Ph.D. Thesis, RWTH Aachen University, Aachen, Germany, 2020.
33. Schloffer, M.; Rashkova, B.; Schöberl, T.; Schwaighofer, E.; Zhang, Z.; Clemens, H.; Mayer, S. Evolution of the ω phase in a β -stabilized multi-phase TiAl alloy and its effect on hardness. *Acta Mater.* **2014**, *64*, 241–252. [[CrossRef](#)]
34. Bolz, S. Eigenschaftsoptimierung und Prozessfensterbestimmung der γ -TiAl-Schmiedelegerung TNB-V4. Ph.D. Thesis, Universität Cottbus, Senftenberg, Germany, 2015.
35. Clemens, H.; Schretter, P.; Glatz, W. Mikrostruktur und Eigenschaften von gamma-TiAl-Basislegierungen. *Prakt. Metallogr.* **1996**, *33*, 17–35.
36. Jones, S.A.; Kaufman, M.J. Phase equilibria and transformations in intermediate titanium-aluminum alloys. *Acta Metall. Mater.* **1993**, *41*, 387–398. [[CrossRef](#)]
37. Lefebvre, W.; Menand, A.; Loiseau, A. Influence of oxygen on phase transformations in a Ti-48 At. pct Al alloy. *Metall. Mater. Trans. A* **2003**, *34*, 2067–2075. [[CrossRef](#)]
38. Ding, H.; Nie, G.; Chen, R.; Guo, J.; Fu, H. Influence of oxygen on microstructure and mechanical properties of directionally solidified Ti-47Al-2Cr-2Nb alloy. *Mater. Design* **2012**, *41*, 108–113. [[CrossRef](#)]
39. Zollinger, J.; Lapin, J.; Daloz, D.; Combeau, H. Influence of oxygen on solidification behaviour of cast TiAl-based alloys. *Intermetallics* **2007**, *15*, 1343–1350. [[CrossRef](#)]
40. Lamirand, M.; Bonnentien, J.-L.; Ferrière, G.; Guérin, S.; Chevalier, J.-P. Relative effects of chromium and niobium on microstructure and mechanical properties as a function of oxygen content in TiAl alloys. *Scr. Mater.* **2007**, *56*, 325–328. [[CrossRef](#)]
41. Beschliesser, M.; Chatterjee, A.; Lorich, A.; Knabl, W.; Kestler, H.; Dehm, G.; Clemens, H. Designed fully lamellar microstructures in a γ -TiAl based alloy: Adjustment and microstructural changes upon long-term isothermal exposure at 700 and 800°C. *Mater. Sci. Eng. A* **2002**, *329*, 124–129. [[CrossRef](#)]
42. Schwaighofer, E.; Schloffer, M.; Schmoelzer, T.; Mayer, S.; Lindemann, J.; Guether, V.; Klose, J.; Clemens, H. Influence of Heat Treatments on the Microstructure of a Multi-Phase Titanium Aluminide Alloy. *Pract. Metallogr.* **2012**, *2012*, 124–137. [[CrossRef](#)]
43. Qin, G.W.; Oikawa, K.; Sun, Z.M.; Sumi, S.; Ikeshoji, T.; Wang, J.J.; Guo, S.W.; Hao, S. Discontinuous Coarsening of the Lamellar Structure of γ -TiAl-based Intermetallic Alloys and Its Control. *Metall. Mater. Trans. A* **2001**, *2001*, 1927–1938. [[CrossRef](#)]
44. Gabrisch, H.; Lorenz, U.; Pyczak, F.; Rackel, M.W.; Stark, A. Morphology and stability of orthorhombic and hexagonal phases in a lamellar γ -Ti-42Al-8.5Nb alloy—A transmission electron microscopy study. *Acta Mater.* **2017**, *135*, 304–313. [[CrossRef](#)]
45. Rackel, M.W.; Stark, A.; Gabrisch, H.; Schell, N.; Schreyer, A.; Pyczak, F. Orthorhombic phase formation in a Nb-rich γ -TiAl based alloy—An in situ synchrotron radiation investigation. *Acta Mater.* **2016**, *121*, 343–351. [[CrossRef](#)]
46. Aguilar, J.; Schievenbusch, A.; Kätzlitz, O. Investment casting technology for production of TiAl low pressure turbine blades—Process engineering and parameter analysis. *Intermetallics* **2011**, *19*, 757–761. [[CrossRef](#)]
47. Sizova, I.; Sviridov, A.; Bambach, M.; Eisentraut, M.; Hemes, S.; Hecht, U.; Marquardt, A.; Leyens, C. A study on hot-working as alternative post-processing method for titanium aluminides built by laser powder bed fusion and electron beam melting. *J. Mater. Process. Technol.* under review.

48. Löber, L.; Biamino, S.; Ackelid, U.; Sabbadini, S.; Epicoco, P.; Fino, P.; Eckert, J. Comparison of selective laser and electron beam melted titanium aluminides. In Proceedings of the Conference Paper of 22nd International Solid Freeform Fabrication Symposium, Austin, TX, USA, 8–10 August 2011; pp. 547–556.
49. Schwerdtfeger, J.; Körner, C. Selective electron beam melting of Ti–48Al–2Nb–2Cr: Microstructure and aluminium loss. *Intermetallics* **2014**, *49*, 29–35. [[CrossRef](#)]



© 2020 by the authors. Licensee MDPI, Basel, Switzerland. This article is an open access article distributed under the terms and conditions of the Creative Commons Attribution (CC BY) license (<http://creativecommons.org/licenses/by/4.0/>).